Performance evaluation of hyperspectral detection algorithms for sub-pixel objects

Performance evaluation of hyperspectral detection algorithms for sub-pixel objects

R.S. DiPietro[a], D. Manolakis[b], R. Lockwood[b], T. Cooley[c] and J. Jacobson[d]

[a]Northeastern University, 360 Huntington Avenue, Boston, MA 02115
[b]MIT Lincoln Laboratory, 244 Wood Street, Lexington, MA 02420
[c]Space Vehicles Directorate Air Force Research Laboratory
2251 Maxwell Avenue, Kirtland AFB, NM 87117
[d]National Air and Space Intelligence Center, Wright-Patterson AFB, OH 45433

ABSTRACT

One of the fundamental challenges for a hyperspectral imaging surveillance system is the detection of sub-pixel objects in background clutter. The background surrounding the object, which acts as interference, provides the major obstacle to successful detection. Two additional limiting factors are the spectral variabilities of the background and the object to be detected. In this paper, we evaluate the performance of detection algorithms for sub-pixel objects using a replacement signal model, where the spectral variability is modeled by multivariate normal distributions. The detection algorithms considered are the classical matched filter, the matched filter with false alarm mitigation, the mixture tuned matched filter and the finite target matched filter. These algorithms are compared using simulated and actual hyperspectral imaging data.

Keywords: Hyperspectral imaging, target detection, false alarm mitigation

1. INTRODUCTION

The detection of materials and objects using remotely sensed spectral information has many military and civilian applications. Hyperspectral imaging sensors measure the spectrum of each pixel in a two-dimensional image at hundreds of very narrow spectral wavelength (color) bands; the result is a 3D data cube with two spatial and one spectral dimensions. This high-resolution spectral data can be used to detect and identify spatially resolved or unresolved objects based on their spectral signatures. If each material had a unique spectrum, the solution of detection and identification problems would be straightforward. Unfortunately, variabilities in material composition and atmospheric propagation, in addition to sensor noise, introduce random spectral variability into the data cube. In addition, for pixels with unresolved objects, the measured spectrum is a mixture of the object and background spectra. Every detection algorithm must then overcome two major obstacles: spectral variability and background interference. A large number of hyperspectral detection algorithms have been developed and used over the last two decades.[1–4] A partial list includes the classical matched filter, RX anomaly detector, orthogonal subspace projector, adaptive cosine estimator, finite target matched filter, mixture tuned matched filter, subspace detectors, kernel matched subspace detectors and joint subspace detectors. In addition, different methods for dimensionality reduction, background clutter modeling, end member selection and the choice between radiance versus reflectance domain processing multiply the number of detection algorithms yet further.

The purpose of this paper is threefold. First, we introduce a matched filter algorithm with false alarm mitigation capability. This two-threshold detector provides a simple and straightforward alternative to the ENVI® mixture tuned matched filter detector without any noticeable degradation in performance. Second, we provide a unified theoretical derivation of the matched filter, matched filter with false alarm mitigation, mixture tuned matched filter and finite target matched filter[5] detectors. Finally, we compare the performance of these algorithms with both simulated and real hyperspectral imaging data.

Correspondence to D. Manolakis. E-mail: dmanolakis@ll.mit.edu, telephone: 781-981-0524, fax: 781-981-7271.

Algorithms and Technologies for Multispectral, Hyperspectral, and Ultraspectral Imagery XVI, edited by Sylvia S. Shen, Paul E. Lewis, Proc. of SPIE Vol. 7695, 76951W · © 2010 SPIE
CCC code: 0277-786X/10/$18 · doi: 10.1117/12.850036

The paper is organized as follows. Section 2 provides an overview of a replacement model that is widely used in hyperspectral detection. Section 3 moves on to review the classical matched filter with emphasis on its geometrical interpretation. This allows us to identify a potential cause of matched filter false alarms. In section 4 we introduce the matched filter with false alarm mitigation, a dual-threshold detector designed to eliminate many of the false alarms associated with the standard matched filter. Section 5 then reviews the mixture tuned matched filter, a popular approach to matched filter false alarm mitigation that is found in the ENVI® software environment. The finite target matched filter is reviewed in section 6 and various results using Gaussian data are provided and discussed. Results using actual hyperspectral data are provided for every detector. Finally, in section 7, we provide a summary of our results.

2. SIGNAL MODEL

Here we restrict ourselves to a two-class linear mixing model that is widely used in hyperspectral detection. We assume that the scene consists of a single background-plus-noise class, with spectra described by the random vector $\mathbf{v}$, and that we are interested in detecting an opaque target, with spectra described by the random vector $\mathbf{t}$. This target 'replaces' the background within the scene, and for a given pixel the amount of replacement we observe physically corresponds to the fraction of pixel area that the target occupies. This fraction is referred to as the fill factor a, and each pixel is a random vector described by

$$\mathbf{x} = a\mathbf{t} + (1-a)\mathbf{v}, \quad 0 \le a \le 1. \tag{1}$$

Each class is assumed to be normally distributed, or

$$\mathbf{t} \sim N(\boldsymbol{\mu}_t, \boldsymbol{\Sigma}_t) \quad \text{and} \quad \mathbf{v} \sim N(\boldsymbol{\mu}_b, \boldsymbol{\Sigma}_b). \tag{2}$$

The notation $\mathbf{x} \sim N(\boldsymbol{\mu}, \boldsymbol{\Sigma})$ is used to imply that the probability density function of $\mathbf{x}$ is

$$f(\mathbf{x}) = \frac{1}{(2\pi)^{p/2}|\boldsymbol{\Sigma}|^{1/2}} \exp\Big(-\frac{1}{2}(\mathbf{x}-\boldsymbol{\mu})^T\boldsymbol{\Sigma}^{-1}(\mathbf{x}-\boldsymbol{\mu})\Big), \tag{3}$$

where p, $\boldsymbol{\mu}$ and $\boldsymbol{\Sigma}$ represent the dimensionality, mean and covariance of the class.

In performing sub-pixel detection we are interested in discriminating between two hypotheses. The first is that the pixel under test, $\mathbf{x}$, is composed only of background class $\mathbf{v}$, while the second is that the pixel under test is a linear mixture of $\mathbf{t}$ and $\mathbf{v}$:

$$\begin{aligned} H_0 &: \quad \mathbf{x} = \mathbf{v} \quad &\Rightarrow \quad \mathbf{x} \sim N\Big(\boldsymbol{\mu}_b, \boldsymbol{\Sigma}_b\Big) \\ H_1 &: \quad \mathbf{x} = a\mathbf{t} + (1-a)\mathbf{v} \quad &\Rightarrow \quad \mathbf{x} \sim N\Big(\boldsymbol{\mu}(a), \boldsymbol{\Sigma}(a)\Big), \quad 0 < a \le 1. \end{aligned} \tag{4}$$

Because we assume that the target and background classes are independent, the mixed mean and covariance become

$$\boldsymbol{\mu}(a) = a\boldsymbol{\mu}_t + (1-a)\boldsymbol{\mu}_b \quad \text{and} \quad \boldsymbol{\Sigma}(a) = a^2\boldsymbol{\Sigma}_t + (1-a)^2\boldsymbol{\Sigma}_b. \tag{5}$$

3. THE MATCHED FILTER

The widely used matched filter detector is given by[1]

$$y_{\text{MF}} = \kappa(\boldsymbol{\mu}_t - \boldsymbol{\mu}_b)^T\boldsymbol{\Sigma}_b^{-1}(\mathbf{x} - \boldsymbol{\mu}_b) \tag{6}$$

where κ is a normalization constant. In practice, we set

$$\kappa = \frac{1}{(\boldsymbol{\mu}_t - \boldsymbol{\mu}_b)^T\boldsymbol{\Sigma}_b^{-1}(\boldsymbol{\mu}_t - \boldsymbol{\mu}_b)} \triangleq \frac{1}{\Delta^2} \tag{7}$$

so that the matched filter response is zero when the pixel under test is the background mean ($\mathbf{x} = \boldsymbol{\mu}_b$) and one when the pixel under test is the target mean ($\mathbf{x} = \boldsymbol{\mu}_t$). The quantity Δ^2 is the squared Mahalanobis distance

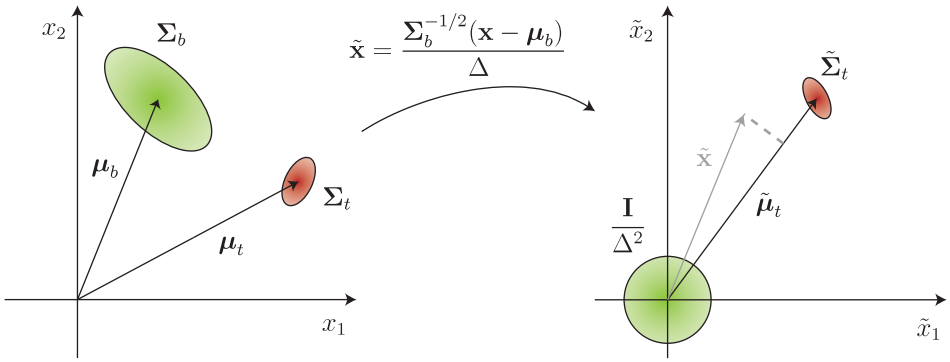

Figure 1. Illustration of the whitening transformation. Also included after the transformation is an example pixel (shown in gray) along with its projection onto the target mean. The matched filter response is the length of this projection.

between the target and background means with respect to the background covariance, and it plays an important role in Gaussian detection. In fact, when observing pixels generated from two Gaussian distributions in the special case $\boldsymbol{\Sigma}_t = \boldsymbol{\Sigma}_b$, the matched filter is the optimal detector and the signal to clutter ratio (SCR) is given by Δ^2. In practice $\boldsymbol{\mu}_b$ and $\boldsymbol{\Sigma}_b$ are estimated from the reflectance data cube while $\boldsymbol{\mu}_t$ is replaced by a library spectral signature $\mathbf{s}$.

We can gain insight into the matched filter by applying the linear transformation

$$\tilde{\mathbf{x}} = T(\mathbf{x}) = \frac{\boldsymbol{\Sigma}_b^{-1/2}}{\Delta}(\mathbf{x} - \boldsymbol{\mu}_b) \tag{8}$$

to our data, as illustrated in figure 1. Under this transformation the background is whitened and centered at the origin. The mean and covariance of the background are given by

$$\tilde{\boldsymbol{\mu}}_b = \frac{\boldsymbol{\Sigma}_b^{-1/2}}{\Delta}(\boldsymbol{\mu}_b - \boldsymbol{\mu}_b) = \mathbf{0} \quad \text{and} \quad \tilde{\boldsymbol{\Sigma}}_b = \frac{\boldsymbol{\Sigma}_b^{-1/2}}{\Delta}\,\boldsymbol{\Sigma}_b\,\frac{\boldsymbol{\Sigma}_b^{-1/2}}{\Delta} = \frac{\mathbf{I}}{\Delta^2} \tag{9}$$

and the mean and covariance of the target are given by

$$\tilde{\boldsymbol{\mu}}_t = \frac{\boldsymbol{\Sigma}_b^{-1/2}}{\Delta}(\boldsymbol{\mu}_t - \boldsymbol{\mu}_b) \quad \text{and} \quad \tilde{\boldsymbol{\Sigma}}_t = \frac{\boldsymbol{\Sigma}_b^{-1/2}}{\Delta}\,\boldsymbol{\Sigma}_t\,\frac{\boldsymbol{\Sigma}_b^{-1/2}}{\Delta} = \frac{1}{\Delta^2}\boldsymbol{\Sigma}_b^{-1/2}\boldsymbol{\Sigma}_t\boldsymbol{\Sigma}_b^{-1/2}. \tag{10}$$

In this space the target mean is a unit vector ($\tilde{\boldsymbol{\mu}}_t^T\tilde{\boldsymbol{\mu}}_t = 1$) and the matched filter takes on the simple form

$$y_{\text{MF}} = \tilde{\boldsymbol{\mu}}_t^T\tilde{\mathbf{x}}, \tag{11}$$

which is the scalar projection of the pixel under test onto the target mean.

In this space it becomes clear that the matched filter only takes the magnitude of the component of $\tilde{\mathbf{x}}$ in the direction of $\tilde{\boldsymbol{\mu}}_t$ into account. It is then possible for a pixel that is very far from any mixture of $\tilde{\boldsymbol{\mu}}_t$ and $\tilde{\boldsymbol{\mu}}_b$ to still receive a high matched filter response. This is a potential cause for matched filter false alarms.

4. THE MATCHED FILTER WITH FALSE ALARM MITIGATION

Here we introduce the matched filter with false alarm mitigation (MF-FAM), a dual-threshold detector with the matched filter response on one axis and a measure of the probability of false alarm on the second axis.

We start by noting that if we could truly obtain the background and target statistics along with the fill factors for every pixel, we could accurately determine each pixel's probability density, which is a relative measure of how likely it is for each pixel to come from its determined mixed distribution:

$$f(\mathbf{x}) = \frac{1}{(2\pi)^{p/2}|\boldsymbol{\Sigma}(a)|^{1/2}}\exp\Big(-\frac{1}{2}\big(\mathbf{x} - \boldsymbol{\mu}(a)\big)^T\boldsymbol{\Sigma}(a)^{-1}\big(\mathbf{x} - \boldsymbol{\mu}(a)\big)\Big). \tag{12}$$

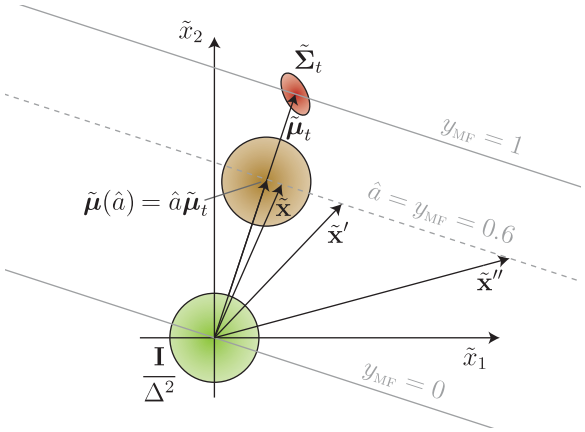

Figure 2. MF-FAM operation in whitened space. Shown are three example pixels that all receive identical matched filter responses. The MF-FAM's second output, the squared Mahalanobis distance from the mixed mean to the pixel under test, is small for $\tilde{\mathbf{x}}$ and large for $\tilde{\mathbf{x}}''$.

Since we're only interested in relative values from pixel to pixel, we can apply monotonic functions and maintain an equally valid measure. By taking the natural log and multiplying by -2 we obtain

$$f'' = \ln|\boldsymbol{\Sigma}(a)| + \big(\mathbf{x} - \boldsymbol{\mu}(a)\big)^T \boldsymbol{\Sigma}(a)^{-1} \big(\mathbf{x} - \boldsymbol{\mu}(a)\big), \tag{13}$$

where the smaller this quantity is the more likely it is that $\mathbf{x}$ came from the mixed distribution.

The first step in making the above equation useful is eliminating any dependence on $\boldsymbol{\Sigma}_t$, as it typically cannot be obtained in practice. We replace $\boldsymbol{\Sigma}(a) = a^2\boldsymbol{\Sigma}_t + (1-a)^2\boldsymbol{\Sigma}_b$ with $\boldsymbol{\Sigma}_b$, which we can obtain a reasonable estimate of. This modification makes the first f'' term constant, and when it is removed we are left with

$$y_{\text{MD}} = \big(\mathbf{x} - \boldsymbol{\mu}(a)\big)^T \boldsymbol{\Sigma}_b^{-1} \big(\mathbf{x} - \boldsymbol{\mu}(a)\big), \tag{14}$$

the squared Mahalanobis distance between the pixel under test and mixed mean with respect to the background covariance. In whitened space this quantity is proportional to squared Euclidean distance, as illustrated in figure 2.

The next and final step is estimating the fill factor a for each pixel. Again avoiding any dependence on $\boldsymbol{\Sigma}_t$, we use the normalized matched filter response as an estimate for a:

$$\hat{a} = y_{\text{MF}}. \tag{15}$$

This estimate is chosen for simplicity and is only equal to the maximum likelihood estimate when 1) an additive (rather than replacement) model is used and 2) the background mean is first subtracted from the data and target signature, so that the scaling parameter behaves like a mixing parameter.

It is interesting to note that the y_{MF}, y_{MD} plane generated by the MF-FAM is almost identical to the y_{MF}, R plane generated by the matched-filter-residual[6] algorithm; R is the square root of y_{MD}. There, y_{MF} and R are derived using a generalized least squares approach and the F statistic. Finally, we note that ROC curves cannot be used to evaluate MF-FAM performance. This is because two thresholds are required for operation, one for y_{MF} and one for y_{MD}.

The data used here and in the following sections for experimental results consists of 255 bands, 159 of which were used for detection. In all cases anomaly detection was performed prior to background estimation to reduce target contamination. The MF-FAM results are shown in figure 3.

We can see that the matched filter alone produces a large number of false alarms. By also thresholding the second axis, the squared Mahalanobis distance from the mixed mean to the pixel under test with respect to the background covariance, many of the false alarms can be eliminated.

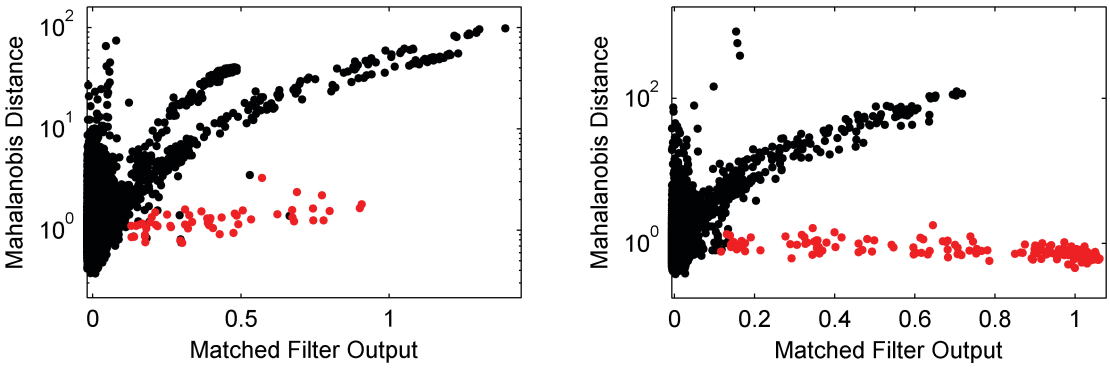

(a) Target 1 (b) Target 2

Figure 3. MF-FAM results using real data. The scene consists of approximately 130,000 background pixels (shown in black), approximately 50 pixels of Target 1 and approximately 150 pixels of Target 2. In each case only the specified target is highlighted red.

5. THE MIXTURE TUNED MATCHED FILTER

The mixture tuned matched filter (MTMF) is a popular approach to matched filter false alarm mitigation and was introduced by Boardman.[8] It can be found in the ENVI® software environment and is a dual-threshold detector that is somewhat similar to the MF-FAM. One axis corresponds to the matched filter response while the other corresponds to what ENVI® refers to as *infeasibility*.

The exact implementation found in the ENVI® environment is not public but here we start by summarizing a derivation given by Schott.[9] This derivation was based on conversation with Boardman and we have found that it gives results that are nearly identical to those given by ENVI®'s implementation. The first step of the algorithm is to determine the noise variability $\mathbf{\Sigma}_N$ of the scene. This part of the algorithm is described in the ENVI® manual. The user must select a subset of the scene that is thought to be as homogeneous as possible, and within this area ENVI® assumes that adjacent pixels contain the same signal but different noise. Vertical and horizontal shift-differences are performed and the resulting 'noise-only' pixels are used to estimate the noise covariance matrix $\mathbf{\Sigma}_N$.

The rest of the algorithm rests on the assumption that the target covariance is equal to the noise covariance. Once this estimate is obtained the data is moved into minimum noise fraction (MNF) space via the transformation

$$T(\mathbf{x}) = \acute{\mathbf{x}} = \left(\mathbf{\Sigma}_N^{-1/2}\mathbf{A}\right)^T\mathbf{x}, \tag{16}$$

where $\mathbf{A}$ is made up of an orthonormal set of eigenvectors of $\mathbf{\Sigma}_N^{-1/2}\mathbf{\Sigma}_b\mathbf{\Sigma}_N^{-1/2}$. This diagonalizes the background and whitens the noise:

$$\acute{\mathbf{\Sigma}}_b = \left(\mathbf{\Sigma}_N^{-1/2}\mathbf{A}\right)^T\mathbf{\Sigma}_b\left(\mathbf{\Sigma}_N^{-1/2}\mathbf{A}\right) = \mathbf{A}^T\mathbf{A}\mathbf{\Lambda}\mathbf{A}^T\mathbf{A} = \mathbf{\Lambda} \tag{17}$$

and

$$\acute{\mathbf{\Sigma}}_N = \left(\mathbf{\Sigma}_N^{-1/2}\mathbf{A}\right)^T\mathbf{\Sigma}_N\left(\mathbf{\Sigma}_N^{-1/2}\mathbf{A}\right) = \mathbf{A}^T\mathbf{I}\mathbf{A} = \mathbf{I}. \tag{18}$$

Here we mention that the MNF transform is usually used prior to dimensionality reduction, in order to retain those axes with the highest signal-to-noise ratio (SNR). However, dimensionality reduction does not take place here, and moving into MNF space shows no apparent benefit.

Next, the data is moved from MNF space to rotated whitened space via the transformation

$$T(\acute{\mathbf{x}}) = \bar{\mathbf{x}} = \frac{\mathbf{\Lambda}^{-1/2}(\acute{\mathbf{x}} - \acute{\boldsymbol{\mu}}_b)}{\Delta}. \tag{19}$$

Here the background is whitened while the noise covariance is diagonalized:

$$\bar{\mathbf{\Sigma}}_b = \frac{\mathbf{\Lambda}^{-1/2}}{\Delta}\mathbf{\Lambda}\frac{\mathbf{\Lambda}^{-1/2}}{\Delta} = \frac{\mathbf{I}}{\Delta^2} \qquad \text{and} \qquad \bar{\mathbf{\Sigma}}_N = \frac{\mathbf{\Lambda}^{-1/2}}{\Delta}\mathbf{I}\frac{\mathbf{\Lambda}^{-1/2}}{\Delta} = \frac{\mathbf{\Lambda}^{-1}}{\Delta^2}. \tag{20}$$

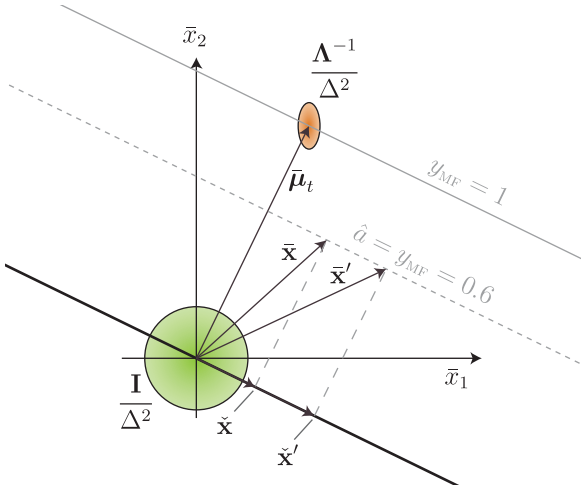

Figure 4. MTMF operation in rotated whitened space. Shown are two example pixels that are projected onto the hyperplane orthogonal to the target mean. The infeasibility of a pixel is its statistical length once projected.

Coordinates in this space are related to those in whitened space (as described in the matched filter section) by an orthogonal transformation (or rotation). The matched filter response is still the projection of the pixel under test onto the target mean:

$$y_{\text{MF}} = \bar{\boldsymbol{\mu}}^T \bar{\mathbf{x}}. \tag{21}$$

At this point Schott states that the projection of a pixel onto the subspace orthogonal to the target mean should tell us how "untarget-like" it is, in the same way that the projection onto the target mean tells use how "target-like" it is. This is illustrated in figure 4. A move to this subspace is made via the transformation

$$T(\bar{\mathbf{x}}) = \check{\mathbf{x}} = \mathbf{P}_t^{\perp} \bar{\mathbf{x}}, \tag{22}$$

where

$$\mathbf{P}_t^{\perp} \triangleq (\mathbf{I} - \bar{\boldsymbol{\mu}}_t \bar{\boldsymbol{\mu}}_t^{\dagger}) \tag{23}$$

is the projection operator and

$$\bar{\boldsymbol{\mu}}_t^{\dagger} \triangleq (\bar{\boldsymbol{\mu}}_t^T \bar{\boldsymbol{\mu}}_t)^{-1} \bar{\boldsymbol{\mu}}_t^T \tag{24}$$

is the pseudoinverse of $\bar{\boldsymbol{\mu}}_t$. We see that in this space both the background and target means are $\mathbf{0}$, and that since ${\mathbf{P}_t^{\perp}}^T = \mathbf{P}_t^{\perp}$ and ${\mathbf{P}_t^{\perp}}^2 = \mathbf{P}_t^{\perp}$, the background and noise covariances are

$$\check{\mathbf{\Sigma}}_b = \mathbf{P}_t^{\perp} \frac{\mathbf{I}}{\Delta^2} \mathbf{P}_t^{\perp} = \frac{\mathbf{P}_t^{\perp}}{\Delta^2} \qquad \text{and} \qquad \check{\mathbf{\Sigma}}_N = \frac{\mathbf{P}_t^{\perp} \mathbf{\Lambda}^{-1} \mathbf{P}_t^{\perp}}{\Delta^2}. \tag{25}$$

The infeasibility measure is defined in this space. It is the statistical length of the pixel under test with respect to the mixed covariance matrix

$$\check{\mathbf{\Sigma}}(a) = a^2 \check{\mathbf{\Sigma}}_N + (1-a)^2 \check{\mathbf{\Sigma}}_b = \frac{a^2 \mathbf{P}_t^{\perp} \mathbf{\Lambda}^{-1} \mathbf{P}_t^{\perp} + (1-a)^2 \mathbf{P}_t^{\perp}}{\Delta^2}, \tag{26}$$

where a is again taken to be the normalized matched filter response. The final result is then

$$y_{\text{INF}} = \check{\mathbf{x}}^T \check{\mathbf{\Sigma}}(a)^{-1} \check{\mathbf{x}}. \tag{27}$$

An important observation prior to implementing the MTMF is that $\check{\mathbf{\Sigma}}(a)$ is necessarily singular. This can be seen by pulling the singular matrix $\mathbf{P}_t^{\perp}$ out of the above expression and noting that a matrix product involving a singular matrix is also singular. This means that we must diagonally load this matrix prior to calculating y_{INF} via

$$\check{\mathbf{\Sigma}}(a, \epsilon) = \check{\mathbf{\Sigma}}(a) + \epsilon \mathbf{I}. \tag{28}$$

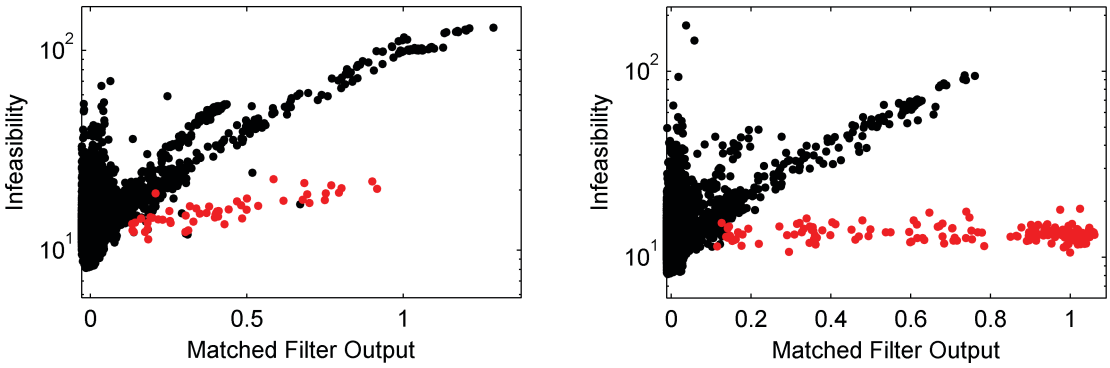

(a) Target 1 (b) Target 2

Figure 5. ENVI® MTMF results using real data. The scene consists of approximately 130,000 background pixels (shown in black), approximately 50 pixels of Target 1 and approximately 150 pixels of Target 2. In each case only the specified target is highlighted red.

The effects of this diagonal loading have not been fully investigated.

We can also see that this algorithm depends heavily on the estimate of the noise covariance matrix. This is problematic because 1) results depend on what area the user chooses as most homogeneous and 2) no homogeneous area may be available for selection, while in this case the shift-difference procedure will produce incorrect results. Finally, there is no evidence that the noise variability describes the target variability well, which is assumed for the remainder of the algorithm.

MTMF results are shown in figure 5. We can see that in this case the ENVI® MTMF performs very similarly to the MF-FAM. This has also been observed with other datasets and in no case have we found the MTMF to outperform the MF-FAM.

6. THE FINITE TARGET MATCHED FILTER

The finite target matched filter (FTMF), which was introduced by Schaum and Stocker,[5] is a single-threshold detector that results from the generalized likelihood ratio test (GLRT). However, unlike the MF and MF-FAM, an estimate of the target covariance is required.

Applying the likelihood ratio test to the hypotheses above yields

$$L = \frac{|\boldsymbol{\Sigma}_b|^{1/2}}{|\boldsymbol{\Sigma}(a)|^{1/2}} \cdot \frac{\exp\Big(-\frac{1}{2}\big(\mathbf{x}-\boldsymbol{\mu}(a)\big)^T \boldsymbol{\Sigma}(a)^{-1}\big(\mathbf{x}-\boldsymbol{\mu}(a)\big)\Big)}{\exp\Big(-\frac{1}{2}\big(\mathbf{x}-\boldsymbol{\mu}_b\big)^T \boldsymbol{\Sigma}_b^{-1}\big(\mathbf{x}-\boldsymbol{\mu}_b\big)\Big)}. \tag{29}$$

Once again, applying monotonic functions does not change performance. By taking the natural logarithm, discarding additive constants and finally removing the scaling factor of 1/2, we obtain

$$y_{\text{FTMF}} = \big(\mathbf{x}-\boldsymbol{\mu}_b\big)^T \boldsymbol{\Sigma}_b^{-1}\big(\mathbf{x}-\boldsymbol{\mu}_b\big) - \big(\mathbf{x}-\boldsymbol{\mu}(a)\big)^T \boldsymbol{\Sigma}(a)^{-1}\big(\mathbf{x}-\boldsymbol{\mu}(a)\big) - \ln|\boldsymbol{\Sigma}(a)|. \tag{30}$$

We can see that when a is fixed we can drop the last term (as it is then constant with respect to $\mathbf{x}$), and in this case the FTMF becomes the well-known quadratic detector. If additionally the background and target statistics are perfectly known then this detector is optimal. However, here we must estimate the background and target statistics as well as the fill factor a for every pixel. The resulting detector is then neither quadratic nor optimal. Sample two-dimensional contour plots are shown in figure 6 for the FTMF, quadratic detector and matched filter.

In order to simplify the estimation of a for each pixel, it is assumed that the background and target statistics have been determined. The maximum likelihood estimate for a is then

$$\hat{a} = \underset{a}{\operatorname{argmax}} \; f\Big(\mathbf{x} \;\Big|\; \boldsymbol{\mu}(a), \boldsymbol{\Sigma}(a)\Big). \tag{31}$$

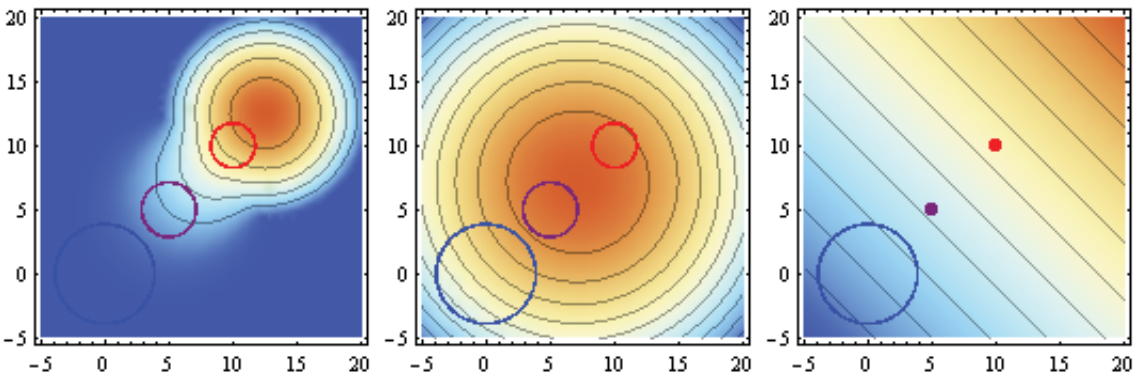

(a) FTMF (b) Quadratic Detector (c) Matched Filter

Figure 6. Detector contours. The blue and red circles represent the background and target distributions respectively, which here are Gaussian with $\boldsymbol{\mu}_b = (0,0), \boldsymbol{\Sigma}_b = 5\mathbf{I}, \boldsymbol{\mu}_t = (10,10)$, and $\boldsymbol{\Sigma}_t = \mathbf{I}$. The purple circles represent the mixed distribution with a fill factor of 0.5. The matched filter does not take the target covariance or mixed covariance into account; this is emphasized by only showing the means of the target and mixed distributions.

Once again applying monotonic functions to the Gaussian density, the function we wish to maximize with respect to a becomes

$$f' = -\frac{1}{2}\ln|\boldsymbol{\Sigma}(a)| - \frac{1}{2}\big(\mathbf{x}-\boldsymbol{\mu}(a)\big)^T\boldsymbol{\Sigma}(a)^{-1}\big(\mathbf{x}-\boldsymbol{\mu}(a)\big). \tag{32}$$

A closed form expression for this maximum is generally not attainable, so for each pixel we must perform optimization or use a brute force method such as trying a set number of a values (e.g., 20) between 0 and 1. However, it is possible to proceed analytically in the special case that the target covariance is proportional to the background covariance. In this case the problem of performing numerical maximization is turned into one of solving a cubic equation, as shown in the appendix. It is necessary to plug 0, 1 and each root found between 0 and 1 into f' to determine the true constrained maximum.

Shown in figure 7 are ROC curves generated using synthetic Gaussian data with $\gamma^2 = 1$. For each target and background class 100,000 samples were generated. Here we are interested in FTMF performance in comparison with optimal detection. This is achievable using the quadratic detector *with knowledge of the fill factor*. Also included are matched filter ROC curves for comparison. Finally, we include FTMF results using both the 'brute force' method of fill factor estimation (labeled FTMF) and the analytic estimation of a as described in the appendix (labeled FTMF*).

When the fill factor is very small, we see equivalent performance among all of the detectors, including the matched filter. This is because when a is very small the mixed covariance matrix is very close to the background covariance, so the matched filter is almost equivalent to the quadratic detector. For mid-range fill factors of 0.30 to 0.70, we see that the quadratic detector and FTMF give much better performance than the matched filter. However, as the fill factor increases, the FTMF performance degrades with respect to the quadratic detector. In the upper limit where $a \to 1$, we can see that the matched filter, which approaches the quadratic detector, outperforms the FTMF.

The FTMF requires an estimate of the target covariance, so for the real dataset each target covariance was modeled as being proportional to that of the background: $\boldsymbol{\Sigma}_t = \gamma^2\boldsymbol{\Sigma}_b$. In addition, dominant mode rejection[7] was performed prior to inversion; the first 80 of 159 eigenvalues were retained. Results are shown in figure 8. Experiments for $\gamma^2 = 0.01$ are not included here, but for both targets performance was only slightly worse than when using $\gamma^2 = 0.1$. We can see that choosing $\gamma^2 = 1.0$ for this dataset diminishes detection performance considerably, while choosing smaller values for γ^2 results in reasonable performance.

7. SUMMARY

In this paper we introduced a matched filter with false alarm mitigation capability and provided its analysis along with that of three other common detectors. An origin of matched filter false alarms was described from

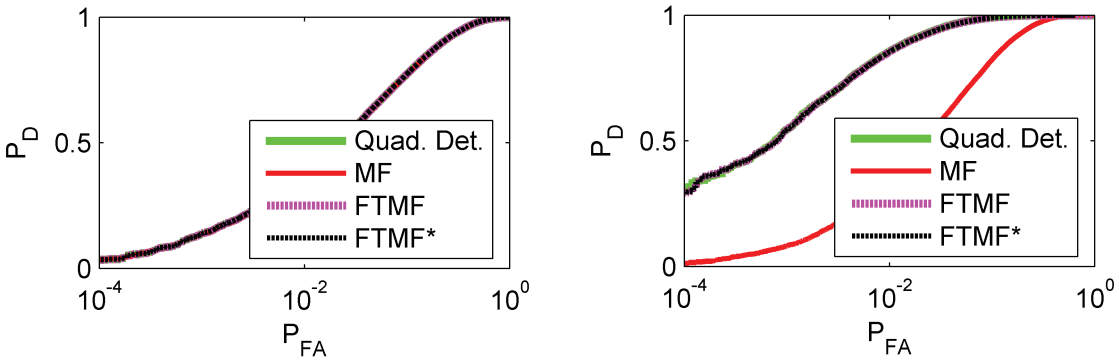

(a) $a = 0.02$ (b) $a = 0.30$

(c) $a = 0.70$ (d) $a = 0.98$

Figure 7. FTMF results using Gaussian data with $p = 50$ bands and $\mathbf{\Sigma}_b = \mathbf{\Sigma}_t = \mathbf{I}$, or $\gamma^2 = 1$. In each case the target mean is chosen so that the Mahalanobis distance between the background mean and *mixed* mean (with respect to the background covariance) is 2.0.

a geometric perspective and this led to the second axis of the MF-FAM, the squared Mahalanobis distance between the mixed mean and pixel under test with respect to the background covariance. Next, the more involved mixture tuned matched filter was analyzed and found to 1) require diagonal loading to invert the covariance matrix projected onto the background subspace and 2) require the specification of a homogeneous area for noise covariance estimation. As a result, the performance changes from user to user. Results between the MF-FAM and MTMF detectors were shown to be similar using a single dataset. Additional datasets have been tested but are not included here; in no case have we seen the MTMF produce better results than the MF-FAM. Finally, the finite target matched filter was described and an analytical estimate for the fill factor was presented in the special case that the target covariance is proportional to the background covariance. Synthetic data was first used to evaluate the FTMF when $\mathbf{\Sigma}_t = \mathbf{\Sigma}_b$. In this case it performed well for small fill factors but was outperformed by the matched filter for large fill factors. Finally, we saw the FTMF perform reasonably well on the real dataset, but that performance depends on the target covariance estimate. Here a proportional model ($\mathbf{\Sigma}_t = \gamma^2 \mathbf{\Sigma}_b$) was used, with $\gamma^2 = 0.1$ giving good results and $\gamma^2 = 1.0$ giving poor results. Choosing γ^2 may be a difficult task in practice.

APPENDIX

Here we derive the closed form solution for the maximum likelihood estimate of the fill factor when the target and background covariance matrices are proportional. In the special case that

$$\mathbf{\Sigma}_t = \gamma^2 \mathbf{\Sigma}_b \tag{33}$$

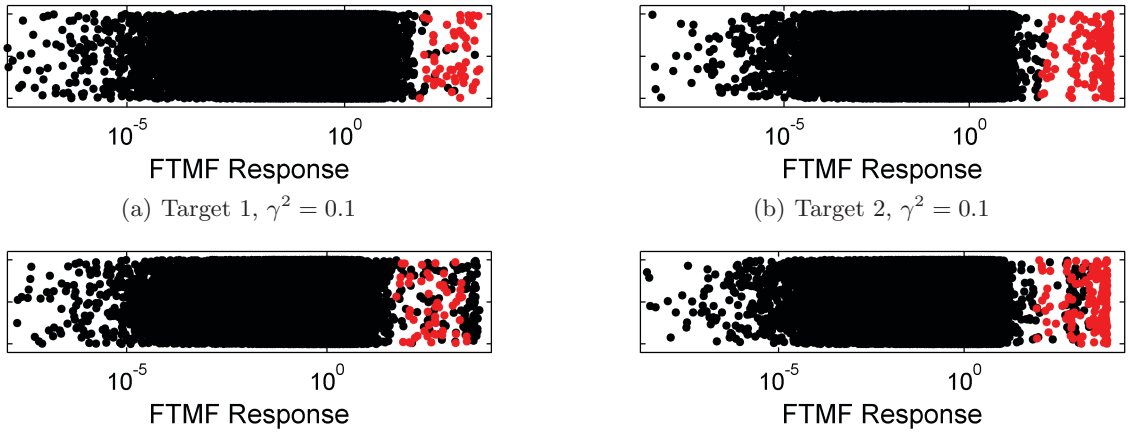

(a) Target 1, $\gamma^2 = 0.1$ (b) Target 2, $\gamma^2 = 0.1$

(c) Target 1, $\gamma^2 = 1.0$ (d) Target 2, $\gamma^2 = 1.0$

Figure 8. FTMF results using real data. Here the vertical axis consists only of random perturbations (for visual separability) and should be ignored. The scene consists of approximately 130,000 background pixels (shown in black), approximately 50 pixels of Target 1 and approximately 150 pixels of Target 2. In each case only the specified target is highlighted red.

the mixed covariance can be written as

$$\mathbf{\Sigma}(a) = a^2\gamma^2\mathbf{\Sigma}_b + (1-a)^2\mathbf{\Sigma}_b = k\mathbf{\Sigma}_b \tag{34}$$

where

$$k \triangleq a^2\gamma^2 + (1-a)^2 \geq 0. \tag{35}$$

This allows us to rewrite the expression we wish to maximize as

$$f' = -\frac{1}{2}\ln|k\mathbf{\Sigma}_b| - \frac{1}{2}k^{-1}\Big(\mathbf{x} - a\boldsymbol{\mu}_t - (1-a)\boldsymbol{\mu}_b\Big)^T\mathbf{\Sigma}_b^{-1}\Big(\mathbf{x} - a\boldsymbol{\mu}_t - (1-a)\boldsymbol{\mu}_b\Big). \tag{36}$$

Now, by rewriting the natural log as

$$\ln|k\mathbf{\Sigma}_b| = \ln|k\mathbf{I}\ \mathbf{\Sigma}_b| = \ln|k\mathbf{I}||\mathbf{\Sigma}_b| = \ln k^p|\mathbf{\Sigma}_b| = p\ln k + \ln|\mathbf{\Sigma}_b|, \tag{37}$$

dropping the constant and multiplying by -2, our problem becomes *minimizing*

$$f'' = p\ln k + k^{-1}\Big(\mathbf{x} - a\boldsymbol{\mu}_t - (1-a)\boldsymbol{\mu}_b\Big)^T\mathbf{\Sigma}_b^{-1}\Big(\mathbf{x} - a\boldsymbol{\mu}_t - (1-a)\boldsymbol{\mu}_b\Big). \tag{38}$$

In order to minimize clutter while taking the derivative with respect to a, we use the notation

$$\delta_{xx} = \mathbf{x}^T\mathbf{\Sigma}_b\mathbf{x}, \quad \delta_{xb} = \mathbf{x}^T\mathbf{\Sigma}_b\boldsymbol{\mu}_b, \quad \text{etc.}, \tag{39}$$

so that f'' becomes

$$f'' = p\ln k + k^{-1}\Big(\delta_{xx} - a\delta_{xt} - (1-a)\delta_{xb} - a\delta_{xt} + a^2\delta_{tt} + a(1-a)\delta_{tb} - (1-a)\delta_{xb} + a(1-a)\delta_{tb} + (1-a)^2\delta_{bb}\Big). \tag{40}$$

By taking the derivative with respect to a, setting it equal to 0 and multiplying both sides of the equation by k^2, we obtain

$$pk\frac{dk}{da} - 2k\Big(\delta_{xt} - \delta_{xb} - \delta_{tb} + \delta_{bb}\Big) + 2ka\Big(\delta_{tt} - 2\delta_{tb} + \delta_{bb}\Big) - \frac{dk}{da}\Big(\delta_{xx} - 2\delta_{xb} + \delta_{bb}\Big) + 2\frac{dk}{da}a\Big(\delta_{xt} - \delta_{xb} - \delta_{tb} + \delta_{bb}\Big) - \frac{dk}{da}a^2\Big(\delta_{tt} - 2\delta_{tb} + \delta_{bb}\Big) = 0. \tag{41}$$

This equation appears to be somewhat daunting but the expressions in parentheses are quite familiar. The first (and fourth) is the matched filter response, the second (and fifth) is the squared Mahalanobis distance between the background and target means with respect to the background covariance, and the third is the anomaly detector response:

$$\begin{aligned} \delta_{xt} - \delta_{xb} - \delta_{tb} + \delta_{bb} &= (\boldsymbol{\mu}_t - \boldsymbol{\mu}_b)^T \boldsymbol{\Sigma}_b^{-1} (\mathbf{x} - \boldsymbol{\mu}_b) \triangleq y_{\text{MF}}, \\ \delta_{tt} - 2\delta_{tb} + \delta_{bb} &= (\boldsymbol{\mu}_t - \boldsymbol{\mu}_b)^T \boldsymbol{\Sigma}_b^{-1} (\boldsymbol{\mu}_t - \boldsymbol{\mu}_b) \triangleq \Delta^2, \\ \delta_{xx} - 2\delta_{xb} + \delta_{bb} &= (\mathbf{x} - \boldsymbol{\mu}_b)^T \boldsymbol{\Sigma}_b^{-1} (\mathbf{x} - \boldsymbol{\mu}_b) \triangleq y_{\text{AD}}. \end{aligned} \tag{42}$$

This leads to the equation

$$pk\frac{dk}{da} - 2ky_{\text{MF}} + 2ka\Delta^2 + 2\frac{dk}{da}ay_{\text{MF}} - \frac{dk}{da}a^2\Delta^2 = 0. \tag{43}$$

Finally, by substituting $\frac{dk}{da} = 2(\gamma^2 + 1)a - 2$ into this equation and laboriously expanding all expressions, we obtain a cubic polynomial in a. The result, after dividing both sides by 2, is

$$Aa^3 + Ba^2 + Ca + D = 0 \tag{44}$$

with

$$\begin{aligned} A &= p(\gamma^2 + 1)^2, \\ B &= (y_{\text{MF}} - 3p)(\gamma^2 + 1) - \Delta^2, \\ C &= -y_{\text{AD}}(\gamma^2 + 1) + p\gamma^2 + 3p + \Delta^2, \\ D &= -p - y_{\text{MF}} + y_{\text{AD}}. \end{aligned} \tag{45}$$

REFERENCES

[1] Manolakis, D., "Taxonomy of detection algorithms for hyperspectral imaging applications," *Optical Engineering* **44**(6), 066403 (2005).

[2] Manolakis, D., Lockwood, R., Cooley, T., and Jacobson, J., "Is there a best hyperspectral detection algorithm?," *Algorithms and Technologies for Multispectral, Hyperspectral, and Ultraspectral Imagery XV* **7334**(1), 733402, SPIE (2009).

[3] Manolakis, D., Marden, D., and Shaw, G., "Target detection algorithms for hyperspectral imaging application," *Lincoln Laboratory Journal* **14**(1), 79–116 (2003).

[4] Schaum, A. P., "Spectral subspace matched filtering," *Algorithms for Multispectral, Hyperspectral, and Ultraspectral Imagery VII* **4381**(1), 1–17, SPIE (2001).

[5] Schaum, A. and Stocker, A., "Spectrally-selective target detection," *Proceedings of ISSSR* (1997).

[6] Foy, B. R., Theiler, J., and Fraser, A. M., "Decision boundaries in two dimensions for target detection in hyperspectral imagery," *Optics Express* **17**(20), 17391 – 17411 (2009).

[7] Manolakis, D., Lockwood, R., Cooley, T., and Jacobson, J., "Hyperspectral detection algorithms: Use covariances or subspaces?," in [*SPIE Annual Meeting*], (2009).

[8] Boardman, J. W., "Leveraging the high dimensionality of aviris data for improved sub-pixel target un- mixing and rejection of false positives: mixture tuned matched filtering," in [*Summaries of the Seventh Annual JPL Airborne Geoscience Workshop*], Green, R. O., ed., **1**, 55, JPL Publication 97-21 (1998).

[9] Schott, J., [*Remote Sensing: The Image Chain Approach*], Oxford University Press, New York, 2nd ed. (2007).

ACKNOWLEDGMENTS

This work was sponsored by the Department of Defense under Air Force Contract FA8721-05-C-0002. Opinions, interpretations, conclusions, and recommendations are those of the author and are not necessarily endorsed by the United States Government.